Decay heat characterization for the European Sodium Fast Reactor

Jiménez-Carrascosa, A.; García-Herranz, N.; Krepel, J.; Margulis, M.; Davies, U.; Shwageraus, E.; Fridman, E.; Gregg, R.;

Originally published:

July 2021

Journal of Nuclear Engineering and Radiation Science 8(2022)1, 011319

DOI: https://doi.org/10.1115/1.4051798

Perma-Link to Publication Repository of HZDR:

https://www.hzdr.de/publications/Publ-32427

Decay heat characterization for the European Sodium Fast Reactor

Antonio JIMÉNEZ-CARRASCOSA
Universidad Politécnica de Madrid (UPM)
José Gutiérrez Abascal, 2, 28006 Madrid, Spain
antonio.jcarrascosa@upm.es

Nuria GARCÍA-HERRANZ
Universidad Politécnica de Madrid (UPM)
José Gutiérrez Abascal, 2, 28006 Madrid, Spain
nuria.garcia.herranz@upm.es

Jiri KREPEL
Paul Scherrer Institut (PSI)
5232 Villigen, Switzerland
jiri.krepel@psi.ch

Marat MARGULIS
Bangor University
Dean St, Bangor LL57 1UT, UK
m.margulis@bangor.ac.uk

Una BAKER
University of Cambridge (UCAM)
Trumpington St, Cambridge CB2 1PZ, UK
ud215@cam.ac.uk

Eugene SHWAGERAUS
University of Cambridge (UCAM)
Trumpington St, Cambridge CB2 1PZ, UK
es607@cam.ac.uk

Emil FRIDMAN
Helmholtz-Zentrum Dresden-Rossendorf (HZDR)
Bautzner Landstraße 400, 01328 Dresden, Germany
e.fridman@hzdr.de

Robert GREGG
National Nuclear Laboratory (NNL)
Chadwick House, Warrington WA3 6AE, UK
robert.wh.gregg@nnl.co.uk

Abstract

In this work a detailed assessment of the decay heat power for the commercial-size European Sodium-cooled Fast Reactor (ESFR) at the end of its equilibrium cycle has been performed. The summation method has been used to compute very accurate spatial- and time-dependent decay heat by employing state-of-the-art coupled transport-depletion computational codes and nuclear data. This detailed map provides basic information for subsequent transient calculations of the ESFR. A comprehensive analysis of the decay heat has been carried out and interdependencies between decay heat and different parameters characterizing the core state prior to shutdown, such as discharge burnup or type of fuel material, have been identified. That analysis has served as a basis to develop analytic functions to reconstruct the spatial-dependent decay heat power for the ESFR for cooling times within the first day after shutdown.

1. Introduction

Sodium-cooled Fast Reactors (SFR) have been identified as the most promising technology among the Generation-IV nuclear systems. With the aim of further improving the safety level of the commercial-size European Sodium Fast Reactor (ESFR), the Horizon 2020 ESFR-SMART project (European Sodium Fast Reactor Safety Measures Assessment and Research Tools) was launched in September 2017 [1]. The ESFR core had been previously developed and investigated in the frame of the CP-ESFR project (Collaborative Project for a European Sodium Fast Reactor) [2] and it is now being optimized in terms of neutronic, thermal-hydraulic and fuel performance [3].

Regarding the neutronics performance, the most recent ESFR core exhibits multiple enhancements compared to previous designs. The assessment of the neutronic behaviour has been carried out within the project for the fresh core [4] along with the characterization of the realistic batch-wise operation [5]. It has led to the definition of the equilibrium core and the characterization of the Beginning of Equilibrium Cycle (BOEC) and End of Equilibrium Cycle (EOEC) states. Along the project, the EOEC core has been selected for further static and transient analyses since it is presented as the most limiting state [6].

Transient analyses require a wide set of parameters as input such as reactivity coefficients, control rod worth or power profiles. In addition, they require a detailed description of the decay heat and its spatial and time dependence following reactor shutdown. The decay heat plays an important role in the design of normal and emergency core cooling systems after shutdown as well as in the design and safety evaluation of spent fuel handling, storage, reprocessing and transportation. A specific task of the ESFR-SMART project is devoted to the assessment of decay heat removal systems following different initiating events [7] identified as the most challenging with respect to the decay heat dissipation capabilities. Therefore, it is crucial to properly characterize the decay heat for the specific ESFR core design to assure the performance of the dedicated safety systems, particularly over the first days following reactor shutdown.

Decay heat is released by decay of radioactive isotopes (both fuel and structural materials) built up along the reactor operation cycle. It is well known that fission products (and nuclides produced by neutron capture by fission products) and actinides are the major contributors [8], while activation products of structural materials play a secondary role in the first days following shutdown. Other source of decay heat, very significant during the first s after reactor shutdown, are fissions induced by delayed neutrons. However, since this term depends on the shutdown reactivity value, it is also generally excluded from decay heat analyses and its contribution is provided by kinetics equations during transient calculations.

Several strategies can be followed for estimating the decay heat in nuclear reactors [9]:

- Traditionally, the so-called decay heat standards have been used. They are a set of tabulated data and exponential functions that fit integral decay heat power obtained from both calculations and experimental data. Most of standards are dedicated to thermal reactors [10], being the Japan Atomic Energy Research Institute (JAERI) standard [11], JAERI-M-91-034, the only one applicable to fast reactors. Although standards are practical for use in system codes for accident analyses, they lie on many assumptions that could lead to significant uncertainties depending on the specific reactor design and its operating conditions [12].
- On the other hand, the so-called summation or explicit calculation method can be applied to compute decay heat. First, an explicit calculation of the isotopic composition of a nuclear system during operation and following shutdown is performed. Then, decay heat power is obtained multiplying the individual decay rate of each nuclide by its corresponding recoverable energy per decay and summing all individual contributions.

The use of standards was imperative in the earlier years of nuclear reactors as decay data for short-lived fission products were scarce. However, as all the required nuclear data (including decay constants, cross sections, fission product yields and recoverable decay energy values) have been available, the summation method has become satisfactory and highly reliable, being nowadays the most extended way to compute decay heat.

In this work the summation method has been used to compute very accurate spatial- and time-dependent decay heat power up to a month after shutdown of the ESFR core at EOEC to be subsequently used by transient codes [13]. Only decay heat from fuel materials is considered.

First, detailed coupled transport-depletion calculations combined with state-of-the-art nuclear data have been performed to provide a reliable estimation of decay heat. Second, a comprehensive analysis of the decay heat has been carried out, identifying the major isotope contributors along with the interdependencies between the variables affecting the decay heat (power before shutdown, discharge fuel burnup, type of fuel material). Then, that analysis has served as a basis to develop analytic functions for the decay heat characterization for cooling times of importance for transient studies up to 1 day after shutdown.

The paper is structured as follows. A brief description of the EOEC ESFR core is presented in Section 2. Section 3 provides information about the employed computational tools. Results, analysis and developed analytic functions are detailed in Section 4. Finally, main conclusions and future work are summarized in Section 5.

2. Description of the ESFR-SMART equilibrium core configuration

This section provides a description of the ESFR core configuration at the equilibrium cycle. Latest design on the ESFR core has been proposed within the ESFR-SMART project [14]. As shown in Figure 1,

the core consists of two main regions, the inner fuel (IF) and the outer fuel (OF), with 216 and 288 fuel sub-assemblies respectively. A single fuel enrichment of around 18% Pu is adopted for both IF and OF regions. Since the ESFR core has been designed to be operated in a six-batch mode, both regions are divided into a six-batch loading pattern. Core reactivity is controlled by 24 control and shutdown devices (CSD) and 12 diverse shutdown devices (DSD). As new implementation, this new design includes 31 corium discharge tubes (CDT) in the periphery of both radial regions for managing accidental scenarios. The active core is surrounded by 3 rings of reflector sub-assemblies and 2 rings of internal spent fuel storage and finally 4 rings of shielding sub-assemblies.

Regarding the axial layout, Figure 2 shows a simplified scheme of the IF and OF sub-assemblies. The main difference between both regions is the height of the fissile regions in order to improve the radial power uniformity. As previously mentioned, a large sodium plenum is introduced above the active core topped by a neutron absorber region. As important assumption, both IF and OF assemblies of every batch are further divided into several regions to account for exposure to different neutron fluxes. The fissile inner region is divided into 5 axial slices while the fertile zone is divided into 3 axial slices. The fissile outer region is also divided into 5 axial slices but the fertile zone is accounted as a single axial slice. Then, the core presents 84 material regions (8 materials in each of 6 batches for IF plus 6 materials in each of 6 batches for OF), which allows the characterization of the relevant core safety parameters with a very high spatial resolution. This batch-wise discretization was proposed in [5], where the equilibrium core state was established, and it was used for the assessment of spatial-dependent reactivity coefficients [6].

The transition from BOEC to EOEC conditions corresponds to a cycle length of 362 days at full power. In this work, aiming at the evaluation of the spatial decay heat distribution at EOEC, the detailed fuel composition at BOEC must be taken as starting point for adequately accounting for the whole inventory. It is also worthy to highlight that the computed decay heat will correspond to an irradiation period prior to shutdown of nearly one year.

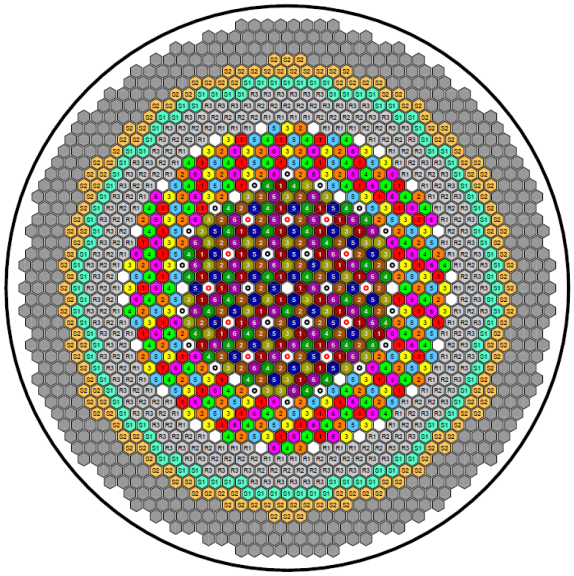

1 2 3 4 5 6	IF SA	6 batches × 36
1 2 3 4 5 6	OF SA	6 batches × 48
	CSD / DSD	24 / 12
R1 R2 R3	Reflector	66 / 96 / 102
S1	Spent IF storage	3 batches × 36
S2	Spent OF storage	3 batches × 48
	CDT	31

Fig. 1 Radial core layout

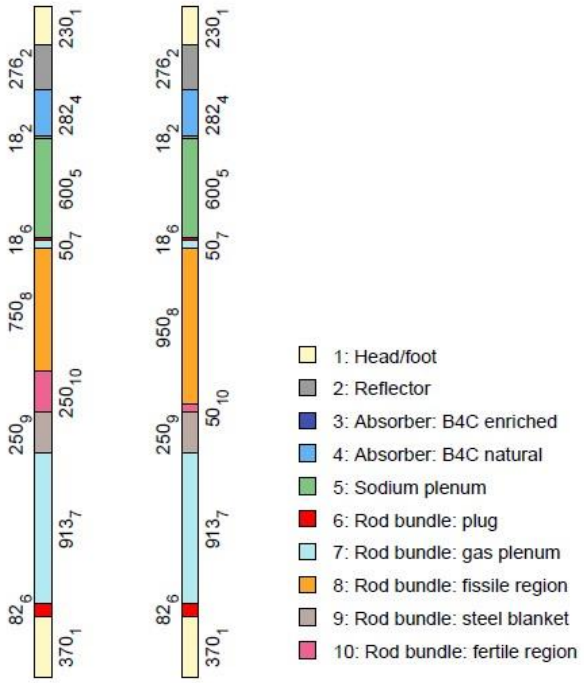

Fig. 2 Axial layout of IF (left) and OF (right) assemblies (length in mm at nominal conditions and subscripts indicate the material located at every region).

3. Computational tools

The explicit decay heat evaluation for the ESFR-SMART core has been performed using the SCALE Code System [15], the Monte Carlo (MC) code Serpent [16] and the deterministic code WIMS [17]. The decay heat calculation procedure is divided into two steps. Firstly, the in-core fuel depletion calculation over the cycle length is carried out in order to account for the whole inventory at EOC. Then, the nuclide decay calculation is performed based on the inventory previously obtained at EOC.

When using both SCALE and Serpent, the heterogeneous full core burnup problem has been solved through coupled continuous-energy Monte Carlo transport-depletion calculations using the Joint Evaluated Fission and Fusion File (JEFF) neutron data library version 3.1 [18].

Serpent includes a built-in decay and depletion solver coupled via the predictor-corrector approach [19]. The decay and transmutation chains are full and constructed automatically without any approximations before every burnup calculation using initial burnable material content. The required radioactive decay and fission yield data is directly read from ENDF-6 (Evaluated Nuclear Data File) formatted JEFF-3.1.1 radioactive decay data file and JEFF-3.1 neutron-induced fission product yields file respectively.

SCALE includes the TRITON sequence, enabling the coupling of KENO-VI and ORIGEN [20] codes using a middle-of-step predictor-corrector approach. ORIGEN is an extensively tested and validated code for decay heat analysis [21–23] which tracks more than 2000 nuclides. The ORIGEN data

resources include: ENDF/B-VII.1 decay data; ENDF/B-VII.0-based fission product yields data and JEFF-3.0/A neutron activation file. In order to accurately consider the nuclides' impact on neutron transport as a function of burnup, a set of 297 nuclides was chosen in this work to be updated in the KENO-VI transport calculations.

Calculations involving the WIMS code suite solved the flux distribution across the core using WIMS-ECCO for initial cross section preparation (JEFF-3.12) and MERLIN for solving for the flux distribution across the core in 33 groups. The latter used a diffusion method with an SP3 approximation. It is important to note that partial nuclide inventories were supplied as part of the benchmark specification and subsequently used in the WIMS calculations. Multi group fluxes (and cross sections) were then prepared using output from the WIMS calculation and incorporated into a pin-wise inventory calculation involving the FISPIN-10 code. Similar to ORIGEN, FISPIN-10 tracks a large number of nuclides (~2000) but uses JEF 2.2 decay and fission product data. To ensure the short lived fission product inventory can be accurately predicted, an artificial burnup step of 5 days was modelled that was sufficiently short so as to not perturb the burnup of the fuel significantly, but sufficient large to allow any short lived fission products present in the fuel immediately following shutdown to reach secular equilibrium.

4. Results

The decay heat distribution of the ESFR-SMART core at EOC has been mapped in time and space for two time periods of interest for transient analyses: the first hour following reactor shutdown, referred to as short-term, and up to 30 days, referred to as mid-term. The decay heat spatial distribution has been obtained taking into account the spatial resolution stated in Section 2, that is, in the 84 burnable regions composing the whole core. Additionally, at the shutdown, the region-wise decay heat (inner and outer fuel of every batch) has been also represented. Isotopes with the major contribution to the decay heat along cooling time are identified. Finally, interdependencies between the involved variables (i.e. decay heat itself, discharge burnup, power before shutdown and core region) are analyzed.

4.1 Spatial- and time-dependent decay heat distribution

The total decay heat predicted by Serpent, SCALE and WIMS-FISPIN is compared in Figures 3 and 4 for the short- and mid-term respectively. Results are presented in terms of percentage of the total thermal power (i.e. 3600 MW_{th}). During the first few s, the decay heat is about 6% of the core thermal power and it decreases along the cooling time. One hour after shutdown, 1.3% of the thermal power is still being generated in the core while. After one month, the decay heat is around 0.17% of the nominal power.

A good agreement among the codes is obtained for both periods. Concerning the values predicted by Serpent and SCALE, the highest deviation is about 1.8% during the short-term and about 3.5% along the mid-term. On the other hand, WIMS-FISPIN appear to underestimate decay heat just after shutdown by approximately 6% compared to Serpent. This is most likely due to a slightly larger number of short-lived fission products considered by SCALE and Serpent (even considering that SCALE and Serpent fission yields data is based on ENDF/B-VII.0 and JEFF-3.1.1 respectively while WIMS-FISPIN employed JEFF-2.2 fission yields). Nonetheless, the deviation between WIMS-FISPIN and Serpent drops to less than 1% after 700 s. In addition, it is important to note that the required burnup calculations from BOEC to EOEC may lead to deviations regarding the isotopic inventory at EOEC.

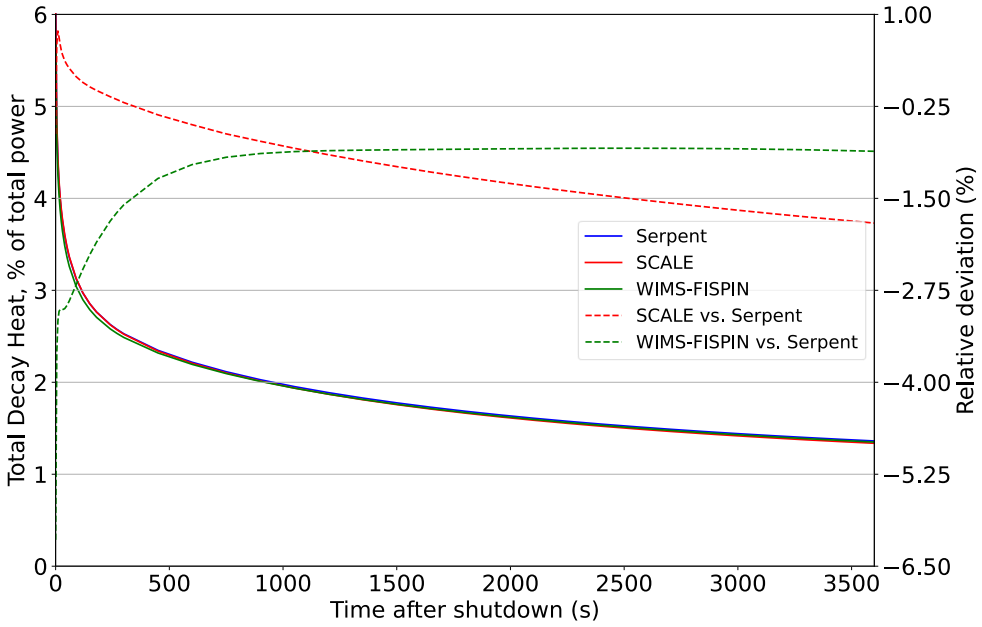

Fig. 3 Total decay heat normalized to nominal power in the short-term.

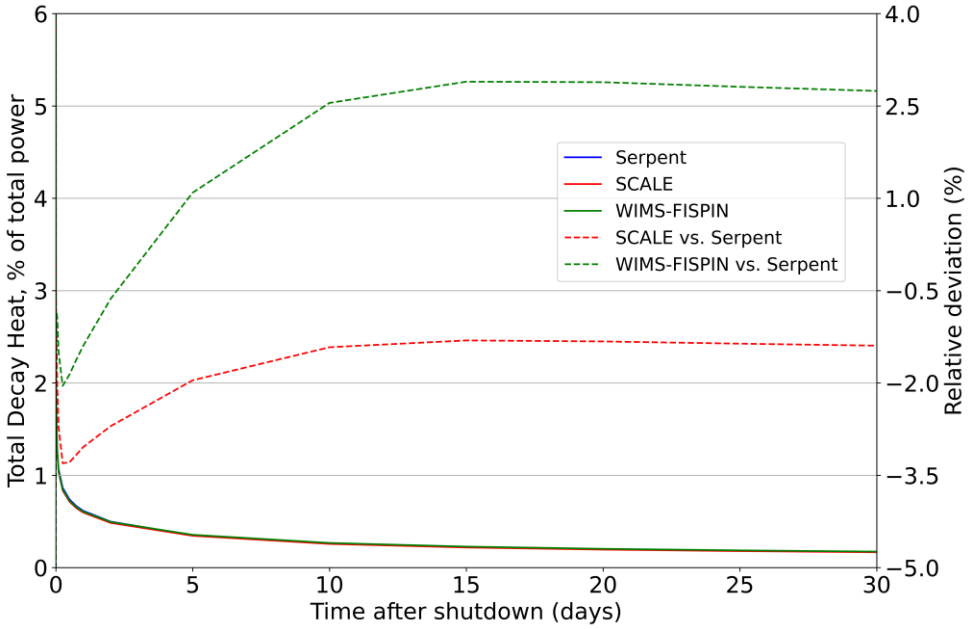

Fig. 4 Total decay heat normalized to nominal power in the mid-term.

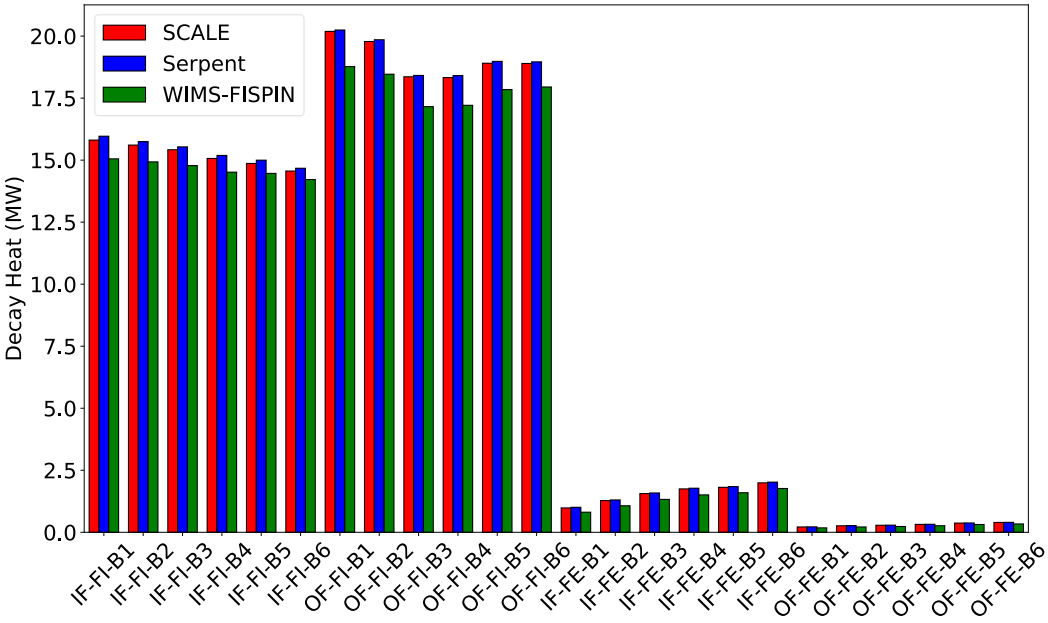

Fig. 5 Zone-wise decay heat distribution just after shutdown.

Transient codes require not only time-dependent values but also the spatial distribution of the decay heat. Figure 5 shows the spatial distribution of the decay heat immediately after shutdown condensed into 24 regions corresponding to the fissile and fertile regions of every batch (6 batches) for both the inner and the outer core.

In this case, SCALE and Serpent agree reasonably well although SCALE systematically predicts a slightly lower decay heat value. Nonetheless, relative deviations do not exceed 2.5% and the highest differences are found for the fertile materials. On the other hand, a higher deviation can be seen between Serpent and WIMS-FISPIN. WIMS-FISPIN systematically underpredicts the decay heat as it was already mentioned.

The fissile zones of the outer core exhibit the highest values of decay heat while fertile regions exhibit the lowest values, following the power distribution at EOEC shown in [5]. The decay heat is then perfectly correlated with the power distribution in the core: the lower the power at EOC, the lower the decay heat immediately after shutdown. This result can be explained keeping in mind that immediately after shutdown the total decay heat is dominated by a large number of short-lived fission products with very short half-lives compared with the irradiation time. As a result, those nuclides have saturated and their activities have reached an equilibrium value proportional to local power.

Figure 6 and Figure 7 depict respectively the detailed axial decay heat profiles for the inner fuel (IF) and outer fuel (OF) batch-wise just after shutdown. Again, the correlation between the power prior to shutdown and the decay heat can be observed, since these profiles are very similar to power profiles reported in [5].

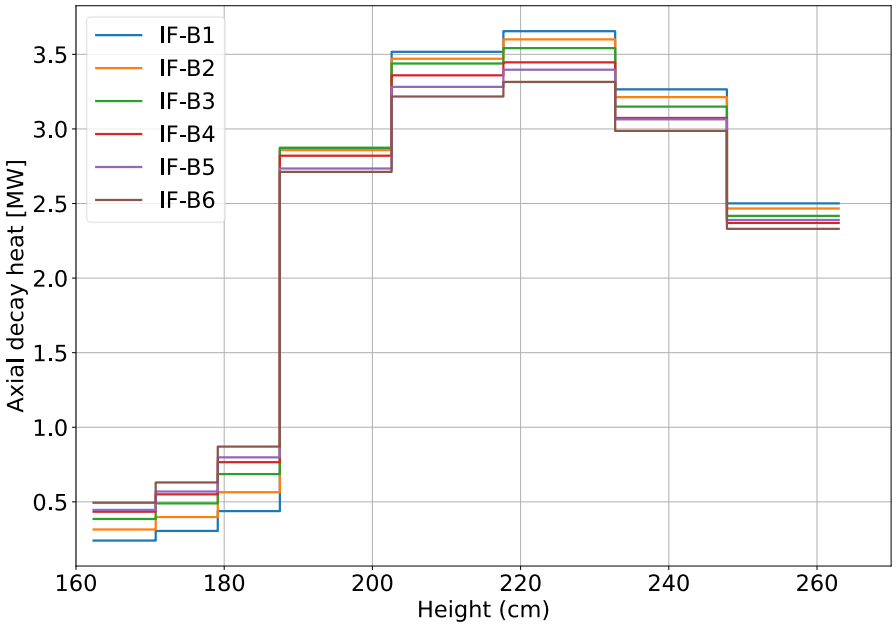

Fig. 6 IF batch-wise axial decay heat profiles just after shutdown.

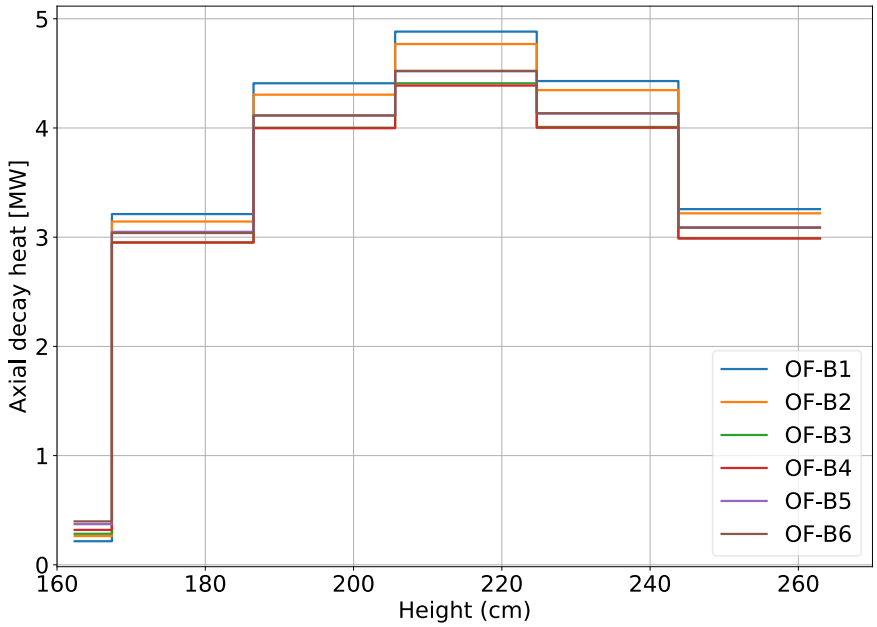

Fig. 7 OF batch-wise axial decay heat profiles just after shutdown.

Regarding the time evolution of the region-wise decay heat, Figure 8 and Figure 9 shows the exponential variation of the normalized decay heat with respect to the initial value for every region in the short- and mid-term respectively. The highest relative decay heat values correspond to the different fertile regions, while all the fissile materials present a very similar evolution. This behaviour will be in-depth analyzed in subsequent sections where the interrelation between all the involved parameters is studied.

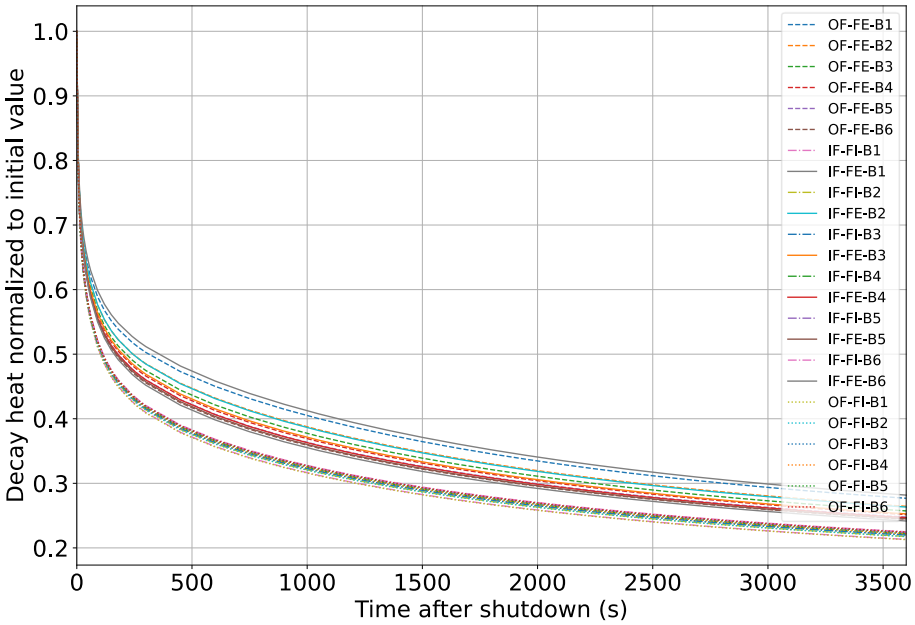

Fig. 8 Zone-wise decay heat evolution normalized to the initial value at the short-term.

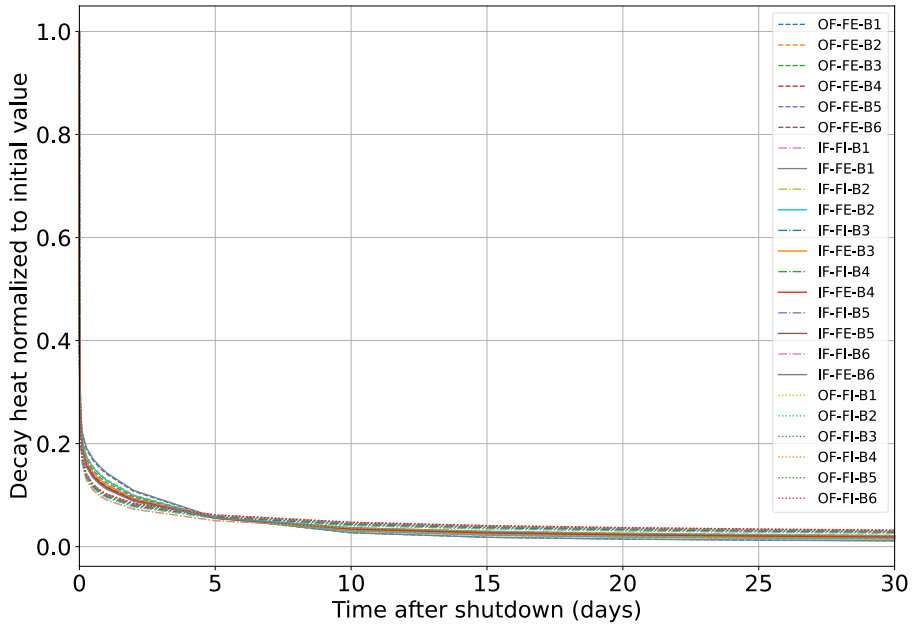

Fig. 9 Zone-wise decay heat evolution normalized to the initial value at the mid-term.

4.2 Major nuclide contributors to the decay heat

The isotopes with the major contribution to the decay heat have been identified for short- and mid-terms (Figure 10).

Actinide contribution to the total decay heat increases from 7% at shutdown to 20% at 30 days. The most relevant actinides are U-239 (its contribution is almost negligible after the first hour), Np-239 (which is the top contributor for times in the range 10 s - 2 days), Cm-242 and Pu-238 (whose importance keeps increasing after one month).

Concerning fission products, during the first 10 s, the 75% of the decay heat is due to a large number (~675) of short-lived fission products with half-lives shorter than 1 h. After one day, about 40 fission fragments dominate the fission product contribution to decay heat (~95%), and after one month, that number falls to only 20 nuclides.

Among the significant nuclides at the short-term period, I-134, Tc-104, Cs-138, La-140, I-132 and I-135. At mid-term, Rh-106, Pr-144, Zr-95, Ru-103 and Nb-95 increase their contribution. These results are consistent with other studies carried out for other SFR cores such as ASTRID [24].

It is crucial to identify the isotopes that are the major decay heat contributors since this response will probably be highly sensitive to nuclear data associated to those nuclides. Then, this preliminary study is the first step for a subsequent uncertainty assessment on the decay heat, which is identified as an activity of interest within the ESFR-SMART project.

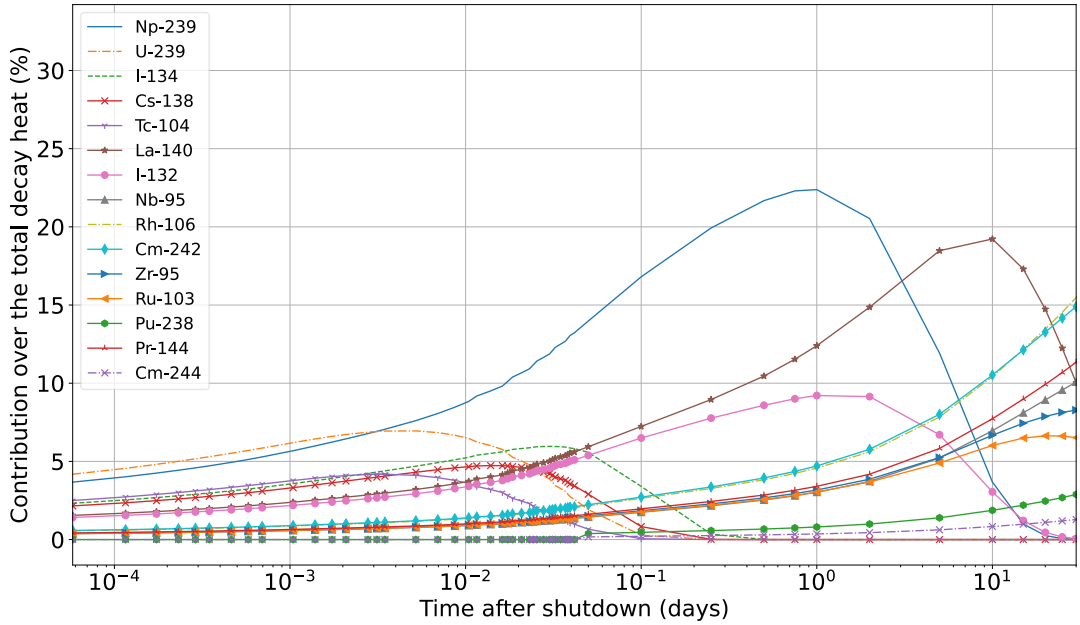

Fig. 10 Major nuclide contributors to the decay heat.

4.3 Analysis of the interdependencies of decay heat and parameters characterizing the core before shutdown

The use of standards to predict decay heat is particularly suitable for safety analysis with system codes. However, as already mentioned, the employed functions should be representative of the specific design under study to provide reliable decay heat power that result in reliable safety-related findings. With the goal of establishing an analytic function able to compute accurate decay heat power distribution for the ESFR core, the interrelations between the decay heat and the different parameters characterizing the ESFR core at EOEC state were analyzed.

After an irradiation period at a certain power level, the state of the core is usually characterized by the axial burnup distribution of fuel assemblies. Interrelations among power before shutdown,

discharge burnup and decay heat have been studied for the 84 burnable materials corresponding to fissile and fertile regions.

The ratio between the decay heat and the power before shutdown has been determined for every material and depicted as a function of the discharge burnup within the short-term (Figure 11) and the mid-term (Figure 12).

At short-term, the following conclusions can be drawn when results for fertile and fissile regions are separated:

- For fissile zones, the ratio does not depend on the discharge burnup and it is mainly affected by the cooling time. This behaviour can be explained by the fact that decay heat at fissile zones is driven by fission products as illustrated in Figure 13 (left), in particular by saturated short-lived fission products, while the contribution of actinides (dominated by Np-239) is much lower. In Figure 14 the U-238 capture rate (responsible of Np-239 generation) divided by total fission rate (responsible of fission products buildup) at EOEC is shown. For fissile regions, such rates are nearly 1:1 and constant with fuel burnup. That is, the split between actinide and fission product composition in the fuel, and therefore their contribution to decay heat, is almost independent on fuel burnup. Consequently, an analytical function to estimate the decay heat of every fissile region might be expected to be only dependent on the power at EOEC and the cooling time.
- For fertile regions, an exponential dependency between the ratio and the discharge burnup can be found. This behaviour can be also understood by focusing on the evolution of U-238, Np-239 and Pu-239. The U-238 capture rate divided by total fission rate for fertile regions is represented in Figure 14. It is worth mentioning that Pu-239 and higher nuclides are absent in fertile fresh fuel and fissions only occur at U-238, so that U-238 capture rate is several times higher than fission rate and actinide component dominate the decay heat production as can be seen in Figure 13 (right). As burnup increases, and thus Pu-239 concentration, the total fission rate swiftly increases in fertile zones, and for a sufficiently high burnup the decay heat is mostly dominated by fission products being its behaviour similar to that of fissile zones (see Figure 13). Consequently, an analytical function to estimate decay heat of every fertile region might be expected to be dependent on the power at EOEC, discharge burnup and cooling time.

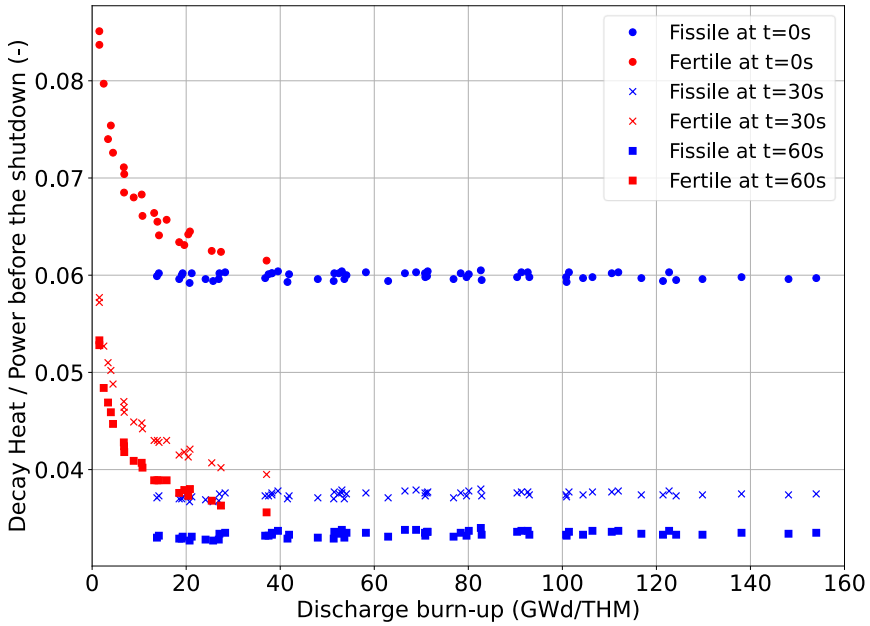

Fig. 11 Ratio between decay heat and power before the shutdown as a function of the discharge burnup for the 84 burnable materials at various cooling times within the short-term.

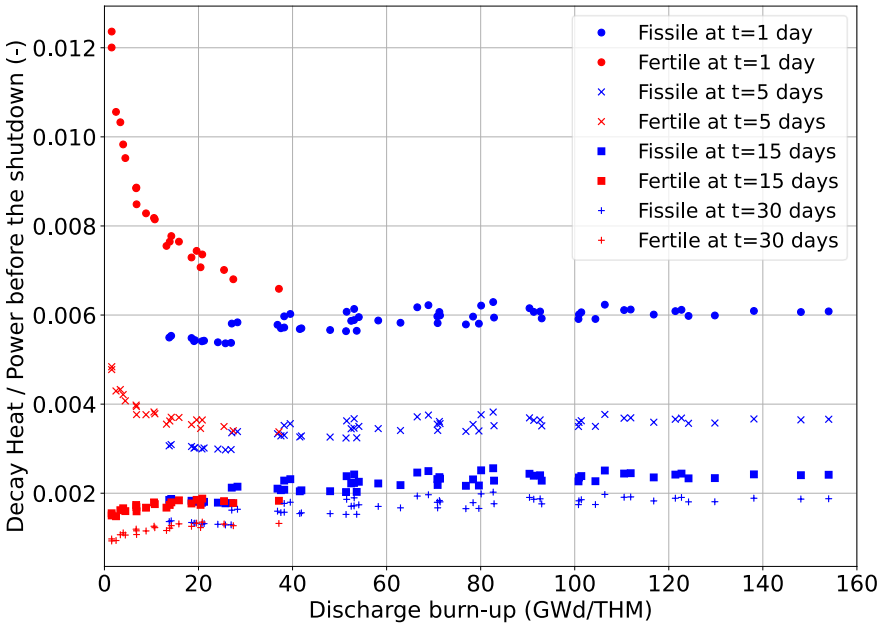

Fig. 12 Ratio between decay heat and power before the shutdown as a function of the discharge burnup for the 84 burnable materials at various cooling times within the mid-term.

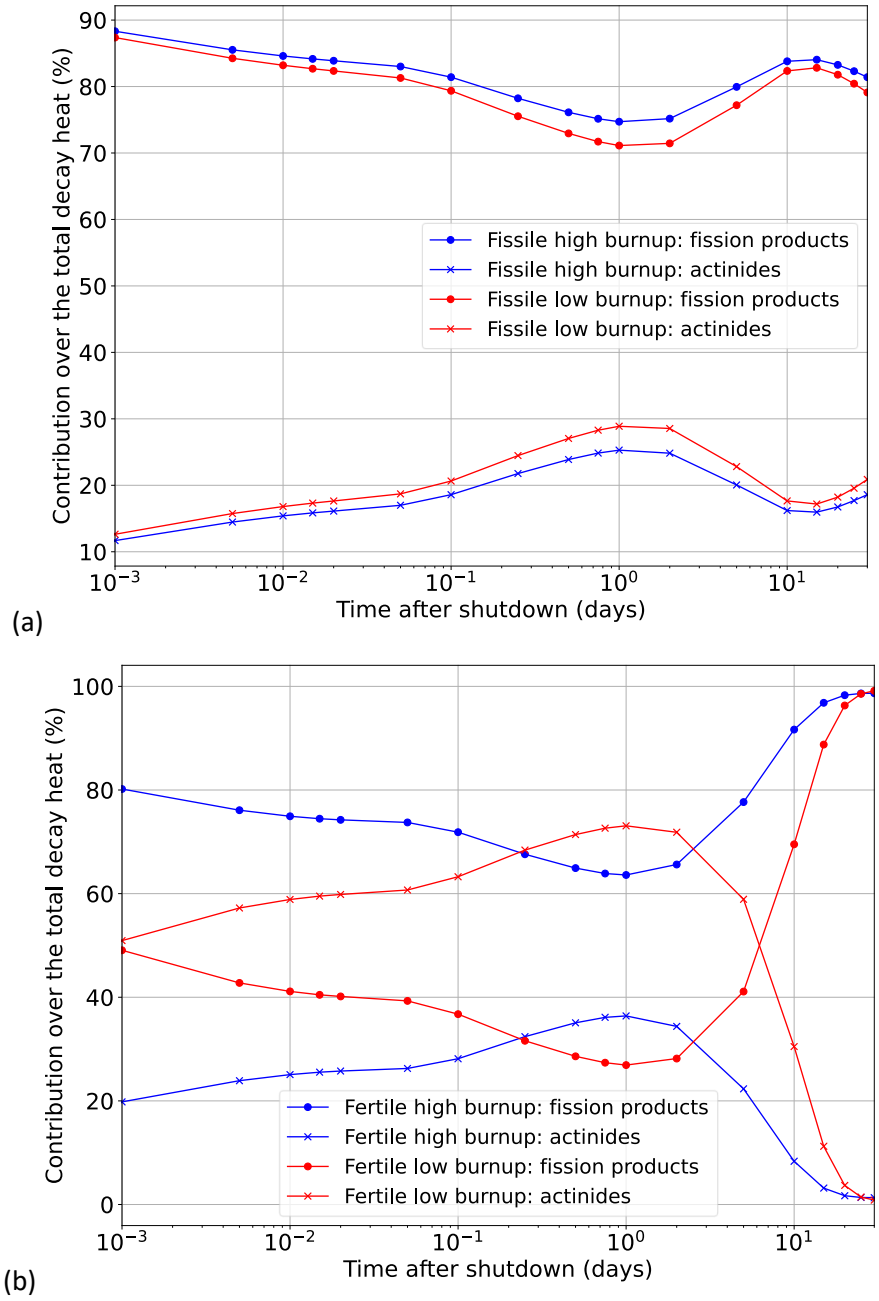

Fig. 13 Fission products and actinides contribution over the total decay heat for (a) fissile and (b) fertile materials at low and high burnup.

At mid-term, patterns represented in Figure 11 are still observed in Figure 12 for both fissile and fertile materials over the first days of cooling. However, for longer times, it can be clearly seen how the behaviour of fertile materials deviates from the trend presented in Figure 11. This is due to the shift in the contribution rate of actinides and fission products to decay heat after few days, illustrated in Figure 13.

Then, analytical functions have been estimated only for the first day following shutdown in order to ensure their applicability to fertile zones of the ESFR. Nonetheless, this time period is sufficiently representative for many typical transient scenarios of this kind of reactors. By properly determining

those analytical functions, it would be possible to compute the decay heat distribution in every required node at each time step directly from readily available parameters at EOEC.

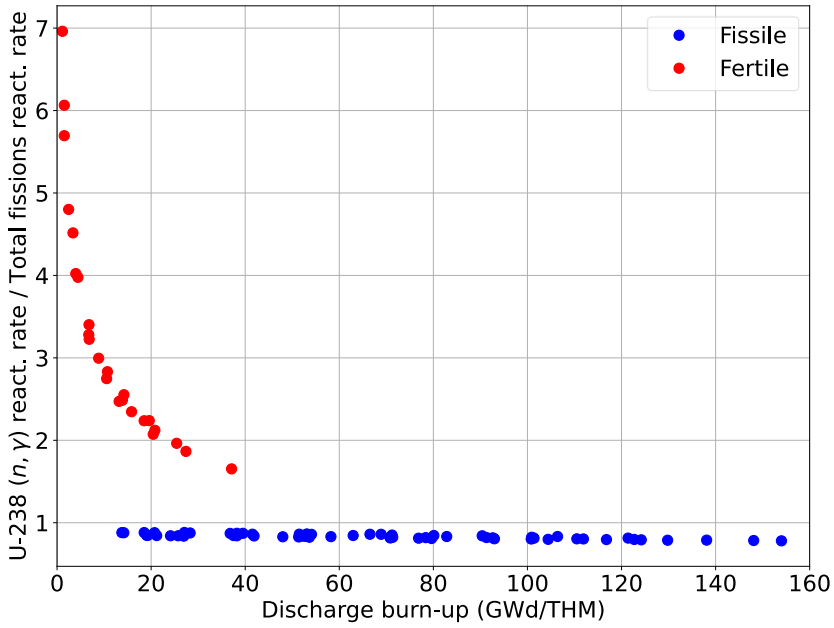

Fig. 14 Ratio of the U-238 capture rate to total fission rate prior to shutdown as a function of discharge burnup for both fissile and fertile zones.

A very simple and widely used formula suggested by Glasstone [25] (Eq. 1) has been selected for this purpose and accordingly fitted using a least-squares approach [26].

$$\frac{P}{P_0} = a \cdot [t^c - (t+b)^c] \tag{1}$$

Where P/P_0 is the dimensionless ratio between the decay heat and the power before shutdown, t is the cooling time (in s) and a, b and c are coefficients to be determined in the subsequent analysis.

The applicability of this function has been divided into two cooling time ranges: from 0 to 150 s after shutdown (the decay heat dramatically decreasing due to the large number of very short-lived fission products), and from 150 s to 1 day. Fitting coefficients a, b and c are presented in Table 1.

Table 1. Coefficients to approximate the ratio P/P_0 depending on both cooling time range and type of material.

	0 to 150 s		150 s to 1 day	
	Fissile	Fertile	Fissile	Fertile
a	-0.012	$-0.012 \cdot BU^{-0.35} - 0.006$	0.524	$0.262 \cdot BU^{-0.46} + 0.802$
b	7.536	$-19.07 \cdot BU^{-0.05} + 22.94$	-0.269	$0.079 \cdot BU^{-0.10} - 0.278$
c	0.816	$0.160 \cdot BU^{-0.11} + 0.727$	0.747	$0.048 \cdot BU^{-0.23} + 0.738$

Concerning fissile regions, Figure 15 shows the evolution of the ratio P/P_0 along cooling time. As already mentioned, there is no strong dependency on discharge burnup and then a single curve can

describe their behaviour. Then, the curve is just depending on cooling time *t* and coefficients *a*, *b* and *c* in Eq. 1 are constants. The performance of this function has been compared against the reference decay heat mapping directly provided by ORIGEN (Figure 16). Regarding the shortest range (i.e. up to 150 s after shutdown), deviations are always lower than 2% showing a very good performance of the analytical function. On the other hand, for cooling time range from 150 s to 1 day, deviations are slightly higher but they are always below 8%.

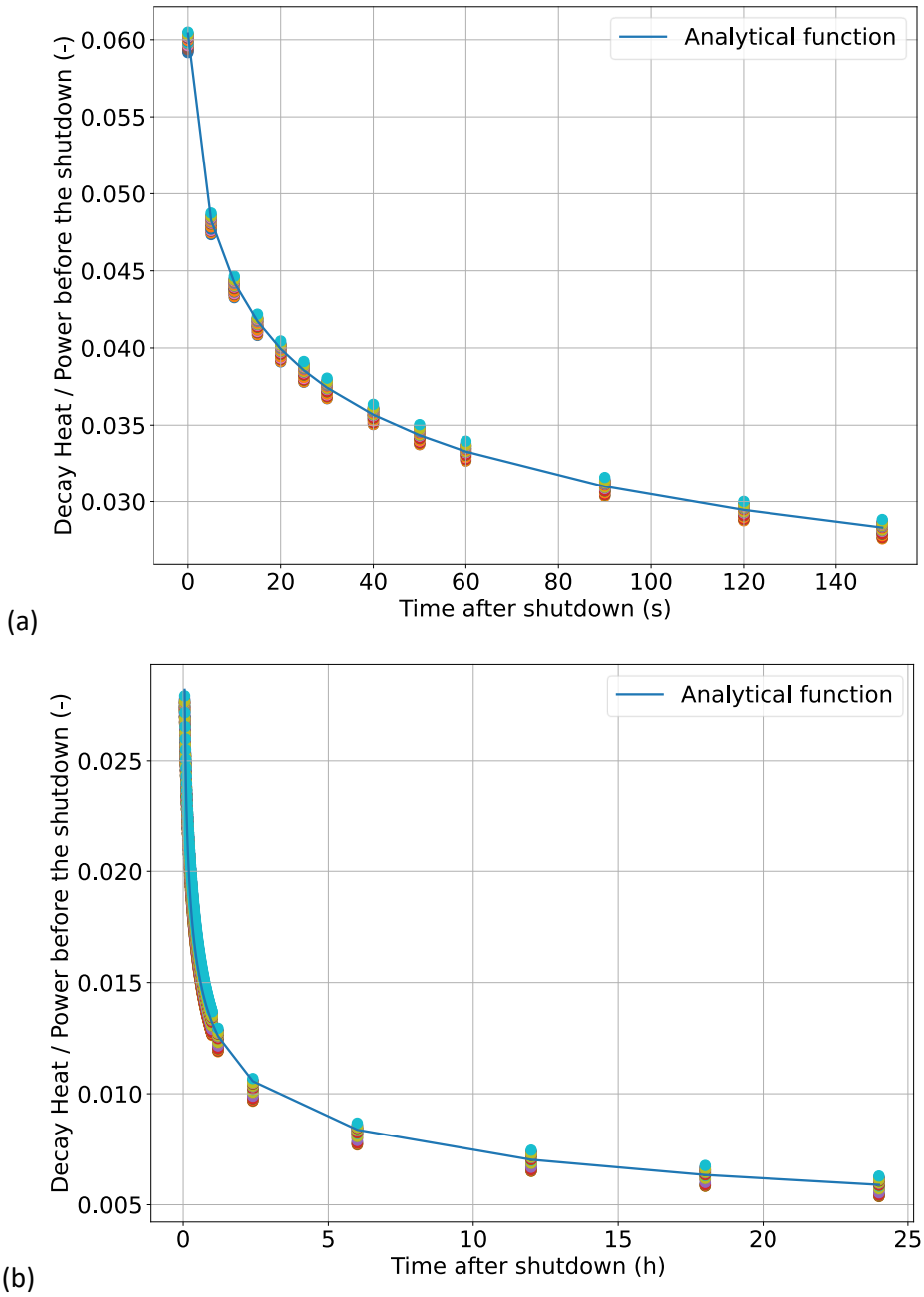

Fig. 15 Ratio between the decay heat and power prior to shutdown for fissile regions along with the derived analytical functions for (a) cooling times up to 150 s and (b) from 150 s to 1 day. Data points represent the ratio between the decay heat and the power for all the fissile burnable regions (i.e., 60 regions in the whole core).

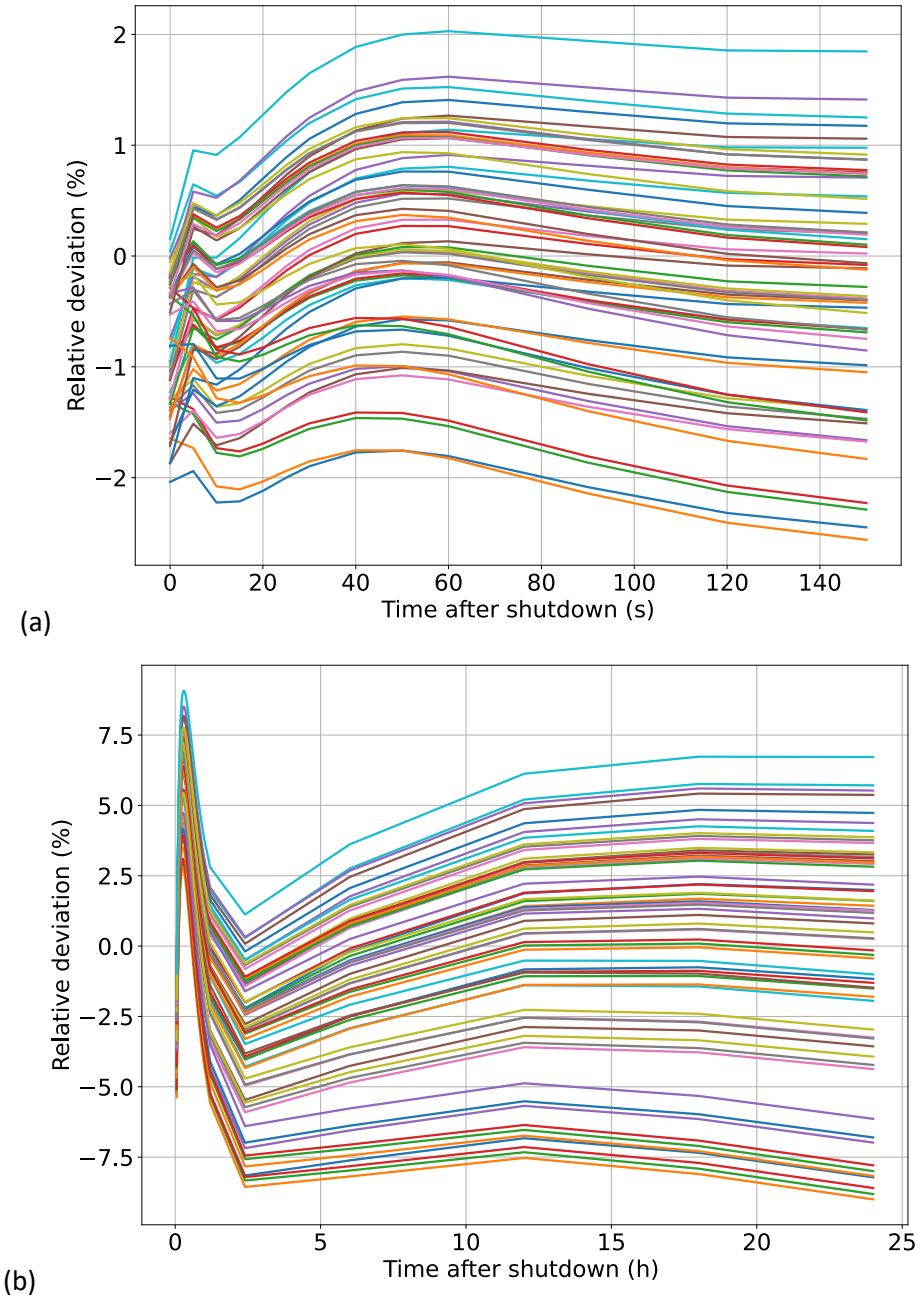

Fig. 16 Fissile regions: relative deviation between reference and estimated function-based decay heat for (a) cooling times up to 150 s and (b) from 150 s to 1 day.

Regarding fertile regions, a more complex formulation is required in order to take into account the dependency of the ratio P/P_0 on the discharge burnup. Thus, coefficients that describe Eq. 1 are dependent on the discharge burnup (*BU*) (in GWd/THM) and have to be corrected in this regard. Figure 17 shows the ratio for the 24 fertile regions involved showing that a single curve is not able to describe the observed behaviour. The performance of the analytical function is also checked for fertile regions. Figure 18 shows the comparison between both the reconstructed and the reference decay heat along the considered cooling time ranges. Along the range which covers up to 150 s after the shutdown, deviations remain below 4%. For cooling times of up to 1 day, differences are again higher observing a

peak where the ratio is still dramatically decreasing. Nonetheless, deviations are mostly lower than 8% along the whole range.

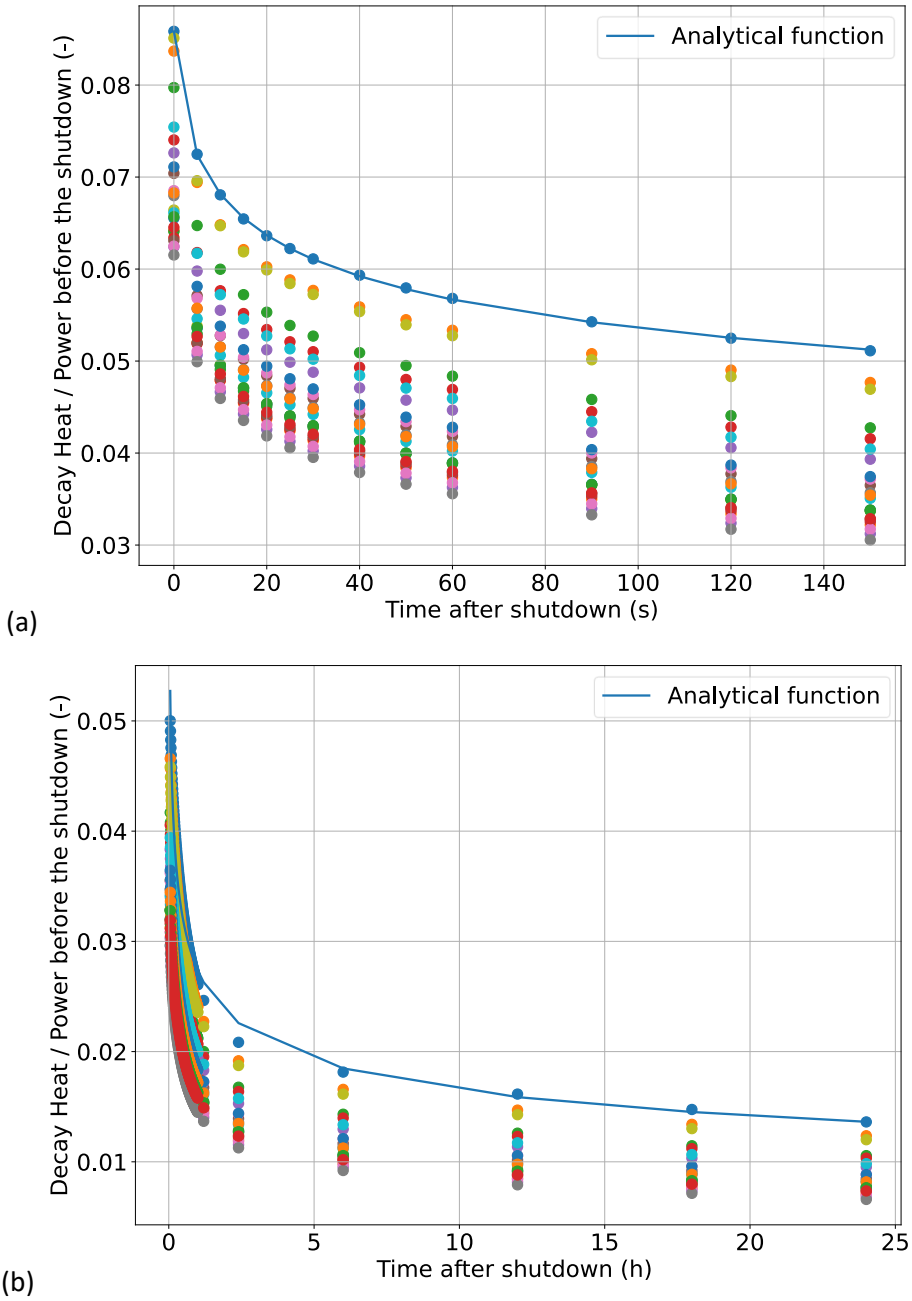

Fig. 17 Ratio between the decay heat and power prior to shutdown for fertile regions along with the derived analytical functions for (a) cooling times up to 150 s and (b) from 150 s to 1 day. Data points represent the ratio between the decay heat and the power for all the fertile burnable regions (i.e., 24 regions in the whole core).

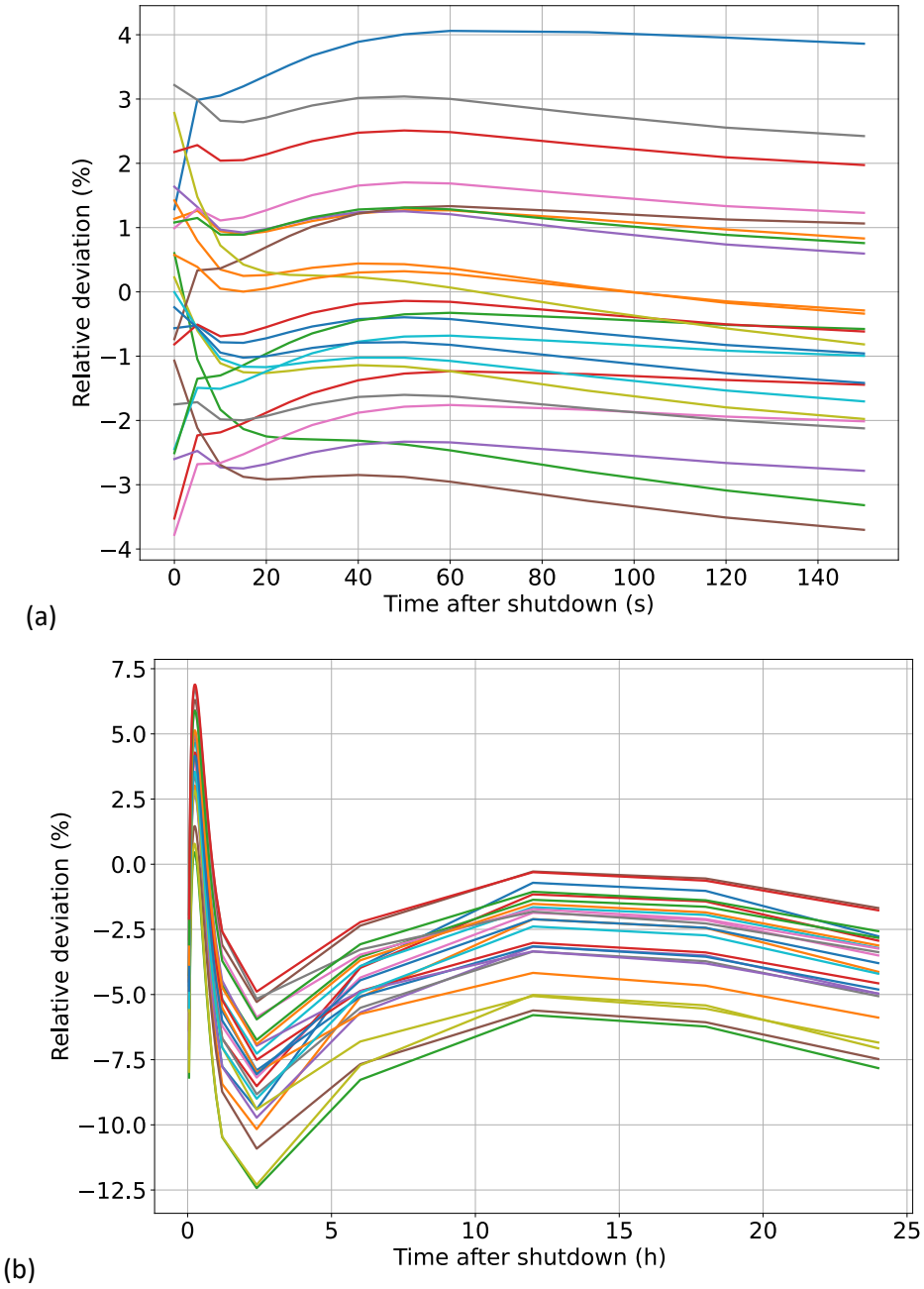

Fig. 18 Fertile regions: relative deviation between reference and estimated function-based decay heat for (a) cooling times up to 150 s and (b) from 150 s to 1 day.

In order to check the general performance of the defined functions, the total decay heat of the ESFR-SMART core has been reconstructed by summing up the region-wise values along both cooling time ranges. Figure 19 shows the performance of the analytical functions compared to the decay heat evolution predicted by ORIGEN. A very good agreement is found for cooling times of up to 150 s, where discrepancies are lower than 0.8% which demonstrates a high accuracy of the function. For the range of up to 1 day, deviations are lower than 2% for cooling times beyond 5 h. During the first hour, an acceptable performance is obtained with deviations lower than 6%.

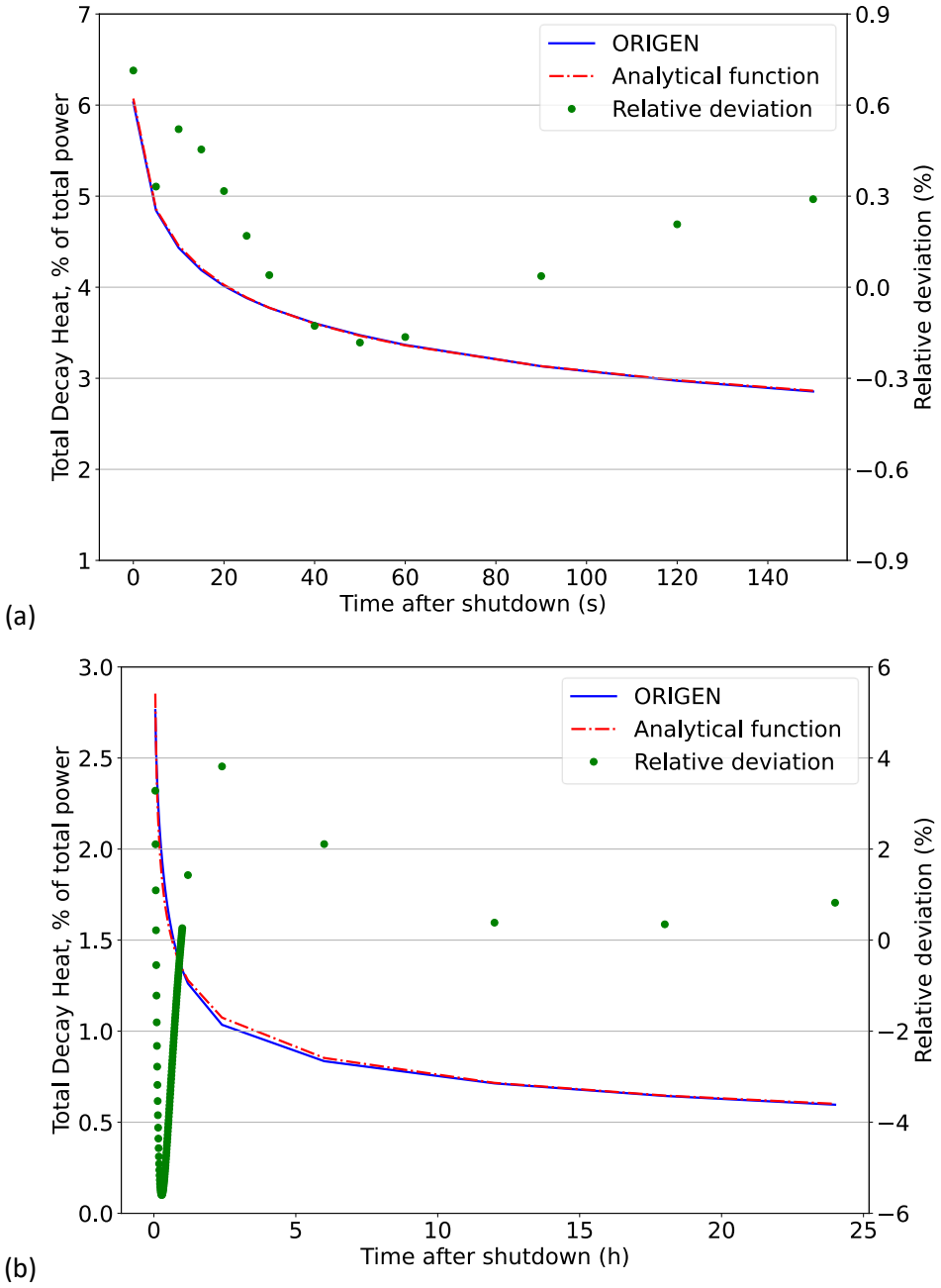

Fig. 19 Total decay heat calculated by ORIGEN compared to the total decay heat estimated by the analytical function for (a) cooling times up to 150 s and (b) from 150 s to 1 day.

5. Summary and conclusions

In this paper a realistic estimation of the decay heat power for cooling times up to a month after shutdown for the recently proposed ESFR core has been performed. Decay heat has been characterized both in space and in time for the subsequent use by transient codes for safety analysis. The decay heat from activation products in structural materials as well as the fission power from delayed neutron have not been considered.

Based on the summation method, the decay heat power has been computed with three different codes widely used along the ESFR-SMART project and state-of-the-art nuclear data libraries. A good

level of agreement is observed between both MC-based codes (i.e. SCALE and Serpent) taking into account that each code carried out an independent transition from BOC to EOC to compute the in-core fuel composition at EOC. Regarding the performance of the deterministic WIMS-FISPIN code, an acceptable agreement is reported with respect to SCALE and Serpent. Deviations are mainly due to the limited number of short-lived fission products considered by WIMS-FISPIN compared to the other codes.

A preliminary study has been also carried out to identify the main isotopes contributing to the decay heat. This is a key exercise towards future work such as the assessment of the impact of nuclear data uncertainties on the decay heat.

Finally, an in-depth analysis of the interrelations between the decay heat power, the fuel composition, power before shutdown and discharge burnup has been performed. That analysis has served as a basis to develop analytic functions to determine the decay heat power for the ESFR for cooling times within the first day following shutdown. It has been observed that the obtained spatial distribution of the decay heat immediately after shutdown is perfectly correlated with the power distribution in the core. For fissile regions, the ratio between decay heat and power before shutdown is independent on the discharge burnup. Then, a simple function has been obtained to predict decay heat for fissile zones just depending on cooling time. On the other hand, for fertile regions, the ratio depends on discharge burnup of subassemblies and a more complex function is proposed.

With those expressions, a very straightforward and accurate determination of the decay heat mapping is possible, only requiring readily available parameters characterizing the core state. Additionally, the performed analysis suggests that a parametrization of decay heat based on U-238 component and Pu vector component in the fuel could be convenient. Ongoing work is focused on the extension of the functions to cover longer cooling times as well as on the assessment of the functions for other ESFR-like fast reactors with similar fuel characteristics.

Funding

The research leading to these results has received funding from the Euratom research and training programme 2014-2018 under Grant Agreement Number 754501 (ESFR-SMART).

Nomenclature

a – fitting coefficient

b – fitting coefficient

BU – Burnup, GWday/$tons_{Heavy\ Metal}$

c – fitting coefficient

P/P_0 – Ratio between the decay heat and the power prior to shutdown

t – cooling time, s

Acronyms and Abbreviations

BOEC – Beginning of Equilibrium Cycle

CDT – Corium Discharge Tubes

CP-ESFR – Collaborative Project for a European Sodium Fast Reactor

CSD – Control and Shutdown Devices

DSD – Dedicated Shutdown Devices

ENDF – Evaluated Nuclear Data File

EOC – End of Cycle

EOEC – End of Equilibrium Cycle

ESFR – European Sodium Fast Reactor

ESFR-SMART – European Sodium Fast Reactor Safety Measures Assessment and Research Tools

FI – Fissile

FE – Fertile

IF – Inner Fuel

JAERI – Japan Atomic Energy Research Insitute

JEFF – Joint Evaluated Fission and Fusion

LWR – Light Water Reactor

MC – Monte Carlo

OF – Outer Fuel

SA – Sub-assembly

SFR – Sodium-cooled Fast Reactor

References

[1] Mikityuk, K., Girardi, E., Krepel, J., Bubelis, E., Fridman, E., Rineiski, A., Girault, N., 2017. ESFR-SMART: new Horizon-2020 project on SFR safety, In Int. Conf. on Fast Reactors and Related Fuel Cycle: Next Generation Nuclear Systems for Sustainable Development (FR17), .

[2] Fiorini, G.L., Vasile, A., 2011. "European Commission – 7th Framework Programme: The Collaborative Project on European Sodium Fast Reactor (CP ESFR)," Nuclear Engineering and Design, vol. 241(9), pp. 3461–3469.

[3] Rineiski, A., Meriot, C., Marchetti, M., Krepel, J., Tsige-Tamirat, H., Álvarez-Velarde, F., Girardi, E., Mikityuk, K., 2022. "New core safety measures and their preliminary assessment in the ESFR-SMART project," Journal of Nuclear Engineering and Radiation Science, vol. 8(1).

[4] Fridman, E., Álvarez-Velarde, F., Romojaro, P., Tsige-Tamirat, H., Jiménez-Carrascosa, A., García-Herranz, N., Bernard, F., Gregg, R., Davies, U., Krepel, J., Massara, S., Poumerouly, S., Girardi, E., Mikityuk, K., 2022. "Neutronic analysis of the European Sodium Fast Reactor: Part I - fresh core results," Journal of Nuclear Engineering and Radiation Science, vol. 8(1).

[5] Fridman, E., Álvarez-Velarde, F., Romojaro, P., Tsige-Tamirat, H., Jiménez-Carrascosa, A., García-Herranz, N., Bernard, F., Gregg, R., Davies, U., Krepel, J., Lindley, B., Massara, S., Poumerouly, S., Girardi, E., Mikityuk, K., 2022. "Neutronic Analysis of the European Sodium Fast Reactor: Part II - Burnup Results," Journal of Nuclear Engineering and Radiation Science, vol. 8(1).

[6] Davies, U., Margulis, M., Shwageraus, E., Fridman, E., Jiménez-Carrascosa, A., García-Herranz, N., Cabellos, O., Gregg, R., Krepel, J., 2022. "Evaluation of the ESFR End of Cycle State: Spatial Distributions of Reactivity Coefficients," Journal of Nuclear Engineering and Radiation Science, vol. 8(1).

[7] Ehster, S., Ammirabile, L., Bubelis, E., Carluec, B., Droin, J.B., Girardi, E., 2022. "Safety Method for the Pre-Conceptual Phase of Sodium-cooled Fast Reactors," Journal of Nuclear Engineering and Radiation Science, vol. 8(1).

[8] Tobias, A., 1980. "Decay heat," Progress in Nuclear Energy, vol. 5(1), pp. 1–93.

[9] Bilodid, Y., Fridman, E., Kotlyar, D., Shwageraus, E., 2018. "Explicit decay heat calculation in the nodal diffusion code DYN3D," Annals of Nuclear Energy, vol. 121, pp. 374–381.

[10] American National Standards Institute/American Nuclear Society, 2014. "ANSI/ANS-5.1 Decay Heat Power in Light Water Reactors," American National Standard, La Grange Park, IL.

[11] Tasaka, K., Katoh, T., Katakura, J., Yoshida, T., Iijima, S., Nakasima, R., Nagayama, S., 1991. "Recommendation on Decay Heat Power in Nuclear Reactors," Journal of Nuclear Science and Technology, vol. 28(12), pp. 1134–1142.

[12] Shwageraus, E., Hejzlar, P., 2009. "Decay heat in fast reactors with transuranic fuels," Nuclear Engineering and Design, vol. 239(12), pp. 2646–2653.

[13] Bodi, J., Ponomarev, A., Bubelis, E., Mikityuk, K., 2022. "Analysis of ESFR decay heat removal systems in Protected Station Blackout," Journal of Nuclear Engineering and Radiation Science, vol. 8(1).

[14] Rineiski, A., Meriot, C., Marchetti, M., Krepel, J., 2018. Core safety measures in ESFR-SMART, In Proc. Int. Conf. PHYSOR 2018, Cancún, México, April 22-26, 9 pages.

[15] Rearden, B.T., Jessee, M.A., 2016. "SCALE Code System," Ornl/Tm-2005/39, (6.2.3), 2747 pages.

[16] Leppänen, J., Pusa, M., Viitanen, T., Valtavirta, V., Kaltiaisenaho, T., 2015. "The Serpent Monte Carlo code: Status, development and applications in 2013," Annals of Nuclear Energy, vol. 82, pp. 142–150.

[17] Lindley, B.A., Hosking, J.G., Smith, P.J., Powney, D.J., Tollit, B.S., Newton, T.D., Perry, R., Ware, T.C., Smith, P.N., 2017. "Current status of the reactor physics code WIMS and recent developments," Annals of Nuclear Energy, vol. 102, pp. 148–157.

[18] OECD/NEA Data Bank, 2016. JEFF-3.1 evaluated data library - neutron data, Free download from: https://www.oecd-nea.org/dbforms/data/eva/evatapes/jeff_31/.

[19] Pusa, M., Leppanen, J., 2010. "Computing the matrix exponential in burnup calculations," Journal of Nuclear Science and Technology, vol. 164, pp. 140–150.

[20] Gauld, I.C., Radulescu, G., Ilas, G., Murphy, B.D., Williams, M.L., Wiarda, D., 2011. "Isotopic depletion and decay methods and analysis capabilities in SCALE," Nuclear Technology, vol. 174(2), pp. 169–195.

[21] Ilas, G., Gauld, I.C., Liljenfeldt, H., 2014. "Validation of ORIGEN for LWR used fuel decay heat analysis with SCALE," Nuclear Engineering and Design, vol. 273, pp. 58–67.

[22] Mirza, S.M., Khan, A., Mirza, N.M., 2010. "Post-shutdown decay power and radionuclide inventories in the discharged fuels of HEU and potential LEU miniature neutron source reactors," Annals of Nuclear Energy, vol. 37(5), pp. 701–706.

[23] Omar, H., Ghazi, N., 2013. "Decay heat analysis of MNSR reactor core using ORIGEN-2 code," Nuclear Engineering and Design, vol. 265, pp. 978–985.

[24] Lebrat, J.F., Vallet, V., Coquelet-Pascal, C., Venard, C., Eschbach, R., 2018. "Uncertainty assessment on the calculated decay heat of the ASTRID basic design core based on the DARWIN-2.3 package," Annals of Nuclear Energy, vol. 120, pp. 378–391.

[25] Glasstone, S., Sesonske, A., 1981. "Nuclear Reactor Engineering," 3rd edition, Van Nostrand Reinhold Company, New York, 820 pages.

[26] The Mathworks Inc., 2020. "Curve Fitting Toolbox: User’s Guide (r2020a)".